Astron. Astrophys. 300,335–345 (1995)

ASTRONOMY AND ASTROPHYSICS

Source counts for the thermal and kinetic Sunyaev–Zel'dovich effects in clusters of galaxies

A. De Luca[1], **F.X. Désert**[1], **and J.L. Puget**[1]

IAS-CNRS, Université Paris XI, Bâtiment 121, F-91405 Orsay Cedex, France

Received 1 September 1994 / Accepted 20 January 1995

Abstract. The growing possibility of observing the thermal and kinetic (Doppler) Sunyaev-Zel'dovich (SZ) sources and their contribution to extragalactic background fluctuations from ground-based and space experiments, scheduled for the next decade, makes it timely to predict source counts as a function of flux. We present calculations of SZ source counts for unresolved cluster of galaxies, including the Doppler effect, and predictions for millimeter and submillimeter wavelengths, not included in previous works. Calculations show that future high sensitivity experiments could observe many thermal and kinetic SZ effect sources in all-sky surveys. The measurement of the kinetic effect on hundreds of clusters could yield precious information on the large scale velocity field of the Universe.

We found a mean Comptonization parameter of $\overline{y} \sim 1.2 \cdot 10^{-6}$, compatible with the COBE limit. We also calculate the contribution of these SZ effect sources to the rms temperature fluctuations relative to the Cosmic Microwave Background and find that it cannot be neglected at small angular scales at a sensitivity level $\delta T/T \sim 10^{-6}$.

Key words: galaxies: clusters of – cosmic microwave background radio continuum: galaxies

1. Introduction

Clusters of galaxies may induce secondary anisotropies in the Cosmic Microwave Background (CMB) by means of gravitational and scattering effects.

Sunyaev & Zel'dovich (1970, 1972; hereafter SZ 1970, SZ 1972) first described the scattering effect and stressed its use as a cosmological tool.

It is possible to identify two main types of SZ distortion. In the *thermal* SZ effect, the inverse-Compton scattering of CMB photons by free hot electrons of the intracluster gas produces a significant spectral distortion in the direction of a cluster: electrons heat up the photons (whose number is conserved), so that CMB intensity appears depleted at lower frequencies ($\nu < 217$ GHz, $\lambda > 1.38$ mm) and increased at higher ones, compared with a line of sight outside of the cluster. The distortion is proportional to the electronic temperature and column density.

The *kinetic* SZ effect is a Doppler distortion due to the peculiar motion of the cluster in the CMB rest-frame and is proportional to the radial component of the peculiar velocity of the cluster and the electronic column density, the spectral signature being identical to primordial CMB anisotropies. Other types of CMB distortions by clusters are indicated in the literature (Sunyaev & Zel'dovich 1980; Vishniac 1987; Birkinshaw 1991), but are much weaker.

Until recently, observations of both effects on single clusters were prohibited by the low brightness of the distortion compared to contamination by other astrophysical sources and systematic errors. Recent improvements in sensitivity (see below), especially at millimetric wavelengths, allow the measurement of the thermal effect on a significant number of clusters and the evaluation of their contribution to anisotropies can be done more accurately. In particular, in the millimeter and centimeter region of the spectrum, SZ sources can contaminate the measurements of primary CMB anisotropies. Predictions of the SZ source counts were therefore conducted taking into account the thermal effect. Korolev et al. (1986), Bartlett & Silk (1994, hereafter BS), Markevitch et al. (1992) and Cavaliere et al. (1993) made similar calculations that we propose to extend to the kinetic effect. Assuming a Press-Schecter mass function for the cluster masses and a gaussian distribution for the cluster radial peculiar velocities, we found that the contribution at all wavelengths of the thermal and the kinetic SZ effect sources to the fluctuations of the CMB is appreciable if a sensitivity of the order of $\delta T/T \sim 10^{-6}$ can be achieved at small angular scales.

1.1. Recent observations

The thermal SZ effect has been observed at radio frequencies (10.7 GHz and 20.3 GHz) with single dish radio telescopes (e.g. Chinbolton Observatory, Birkinshaw et al. 1981a,b; OVRO, Birkinshaw et al. 1984, 1991) on the most favorable candidates, notably the rich Abell clusters A665, A2218 and

Send offprint requests to: A. De Luca

0016+16.

These observations give a one-dimensional profile of the effect through the cluster. To some extent, they are contaminated by systematic uncertainties like confusion induced by radio sources close to the direction of the cluster, fluctuations in atmospheric emission and uncertainties in the zero level of the signal (corresponding to undisturbed CMB). Recently, Jones et al. (1993) and Grainge et al. (1993) realized an interferometric observation with the Ryle Telescope and gave a two dimensional image of the SZ effect on A2218 and A773 at 15 GHz, in which the previous problems have been significantly reduced.

Improvements in the sensitivity of millimetric broad-band receivers and in the efficiency of atmospheric noise removal allowed measurements to be carried out at shorter wavelengths. The SuZIE experiment (Wilbanks et al. 1994; Fischer et al. 1993; Fischer & Lange 1993) has given the first ground-based observation of the SZ effect in the millimeter region (2.2 mm) on A2163, at the peak decrement of the thermal effect, with a small ^{3}He-cooled bolometric array with electronic differential readout operated at the focus of the Caltech Submillimeter Observatory at Mauna Kea. Future observations at 1.2 mm are planned to measure the effect in increment. They estimated the confusion limits to the observations of the thermal and kinetic SZ effects in the millimeter due to radio sources, IR galaxies and Galactic cirrus and found the bands of minimum confusion noise at 3.3 mm for the thermal SZ effect and 2.85 mm for the kinetic SZ effect.

1.2. Future experiments

Several projects dedicated to the observations of the thermal and kinetic SZ effect are being studied or built. Data from ground-based, balloon-borne and satellite experiments will be combined to increase the information in different spectral bands and at different angular scales.

One example of a new generation ground-based experiment is the *DIABOLO* experiment (Désert et al. 1993) which uses bolometers cooled at 100 mK dedicated to the observation of the effects at 1.3 mm and 2 mm for angular scales of 9 arcmin (at the 2.7 m-telescope of Testa Grigia-Cervino, Italy) and of 40 arcsec (at the IRAM-MRT-30 m-telescope of Pico Veleta-Spain). The DIABOLO 3σ sensitivity expected for one hour of integration should be around 10^{-4}, in term of Comptonization parameter y.

The measurement of the positive part of the thermal SZ effect with a beam width of about 3 arcmin and in four channels between 200 and 800 μm is one of the main goals of the balloon-borne experiment *PRONAOS-SPM* (Lamarre et al. 1993; Désert et al. 1993; De Luca et al. 1993; flown for the first time in September 1994, no SZ measurement could be conducted during this flight), a 2 m-telescope coupled to a submillimeter photometer containing ^{3}He-cooled bolometers at 0.3 K. The PRONAOS-SPM expected sensitivity at 3σ for one hour of integration will be $\Delta T/T \sim .10^{-4}$. The results will be coupled to those of DIABOLO experiment, to evaluate the two SZ effects and the contribution of dust emission contamination by means of the shortest wavelength channels.

For the next decade, satellite experiments devoted to the observation of submillimeter backgrounds are studied which would combine the technological advances already used on the ground and in balloons with the low background and large surveyed area allowed by space experiments (e.g. *SAMBA*, Puget 1993; and COBRAS-SAMBA, Mandolesi et al. 1994). In these experiments, a passively cooled 1 m-class telescope with an array of bolometers cooled to 0.1 K is dedicated to the study of CMB anisotropies and the thermal and kinetic SZ effects. They will make observations between 200 μm and 4 mm, on angular scales of 10 arcmin to 10 degrees. The expected 3σ sensitivity will be of $\Delta T/T \sim 3 \times 10^{-6}$ and $y \sim 3 \times 10^{-6}$ per pixel over the whole sky and ten times deeper in limited patches.

With such sensitivities, the contribution of the velocity effect along with the SZ thermal effect to CMB anisotropies cannot be ignored and its evaluation is the main goal of this paper.

1.3. Importance of kinetic SZ effect

The peculiar velocity field of the Universe is most likely determined by the gravitational acceleration that develops from initial density fluctuations in the early Universe (Peebles 1980). It can put strong constraints on the density parameter (Dekel 1993; Bernardeau 1993; see the IAP Conference, 1993) as well as on the primordial spectrum of fluctuations. Up to date simulations (Bahcall et al. 1994) confirm that clusters of galaxies are efficient tracers of the large scale velocity field of the Universe, so that the measurement of their peculiar velocities can give unique information on the velocity field at low redshift and on the cosmological models.

Recently, Lauer & Postman (1994) have compared the Local Group peculiar velocity against the CMB and against distant clusters at $z \leq 0.03$; they found that a coherent velocity field on distance scales larger than $z = 0.03$ must exist. The standard method to measure the peculiar velocity of a source (see, e.g., IAP Conference, 1993) depends on the measurement of its redshift (generally very accurate) and the measurement of its distance (less accurate) given by absolute luminosity indicators: the peculiar velocity is obtained from the difference between these two quantities and becomes very inaccurate for $z > 0.03$. On the other hand, the kinematic SZ effect can give a measure of the radial velocity relatively independent of the distance.

Source counts for the kinetic SZ effect have been neglected in the past because this effect is weaker (by a factor of $3 - 10$) than the thermal SZ effect, but improving sensitivity of future experiments makes it possible to measure the effect on a large number of sources and to consider their contribution to the diffuse astrophysical backgrounds.

2. Integral SZ properties of a cluster

2.1. Thermal SZ effect

The relative brightness variation of CMB at a given frequency ν, observed through an intracluster medium relative to a reference

direction out of the cluster, can be expressed as the product of two separate terms:

$$\frac{\Delta B_{\nu,th}}{B_{\nu,cmb}} = y \cdot f(x). \quad (1)$$

Here $B_{\nu,cmb}$ is the monochromatic brightness of the CMB (Planck law, $T_r = 2.726 \pm 0.010$ K, Mather et al. 1994), $\Delta B_{\nu,th}$ is the change of brightness of the cluster relative to its neighborhood line of sight, y is the *comptonization parameter*, which can be written, assuming the isothermality of the cluster,

$$y = \frac{1}{m_e c^2} \sigma_T \int_l kT_e \, n_e dl = \frac{kT_e}{m_e c^2} \tau \quad (2)$$

[$x = h_p \nu / kT_r$ is the adimensional frequency, T_e is the intracluster gas temperature, $m_e c^2$ is the electron rest mass energy ($0.511\ 10^6$ eV), n_e is the electron plasma density, τ is the optical depth, the integral being made along the line of sight l] and

$$f(x) = x \frac{e^x}{e^x - 1} \left(x \frac{e^x + 1}{e^x - 1} - 4 \right) \quad (3)$$

is a factor characterizing the spectral form of the distortion (the same for all clusters) that depends only on the frequency.

As shown in Fig. 1, $f(x)$ changes in sign at $\nu = 217$ GHz ($x = 3.83$, corresponding to a wavelength $\lambda = 1.38$ mm): as a consequence we will always have *positive* and *negative* SZ sources according to the spectral region which is observed and irrespective of the cluster redshift.

2.2. Kinetic SZ effect

If a cluster has a peculiar motion, with a radial velocity v_r relative to the rest frame of the CMB (which is the natural reference frame to describe the thermal SZ effect), a CMB brightness distortion, depending on the sign of v_r and of exactly the same kind as a primordial anisotropy, will appear due to the Doppler effect

$$\frac{\Delta B_{\nu,kin}}{B_{\nu,cmb}} = -b \cdot a(x). \quad (4)$$

The parameter

$$b = \tau \beta \quad (5)$$

($\beta = v_r / c$) depends only on the cluster peculiar velocity (which is positive for receding clusters) and on the same optical depth τ as in formula (2). The function

$$a(x) = \frac{x \, e^x}{e^x - 1} \quad (6)$$

characterizes the spectral distribution of the kinetic effect and keeps the same sign at all frequencies. In Fig. 1, *SZII* indicates the kinetic effect for a cluster with $b = -10^{-4}$. The brightness temperature variation equivalent to the kinetic effect will be equal to b:

$$\frac{\Delta T_{kin}}{T_{cmb}} = -b. \quad (6')$$

The effect adds linearly with the thermal SZ giving a *total* spectral distortion on CMB at a given frequency:

$$\frac{\Delta B_\nu}{B_{\nu,cmb}} = yf(x) - ba(x). \quad (7)$$

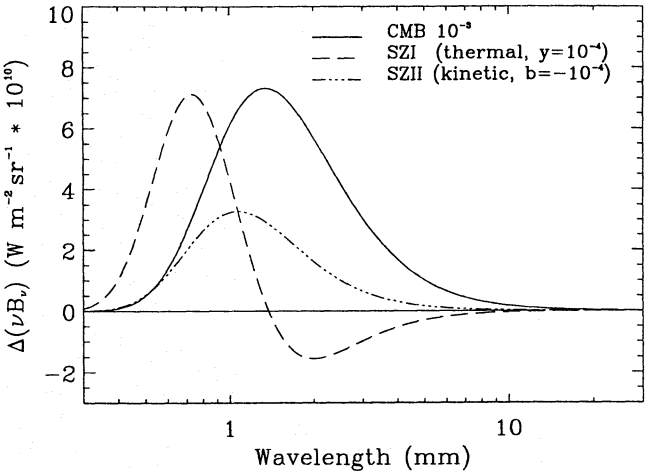

Fig. 1. A cluster SZ distortion brightness as a function of wavelength. CMB is the Cosmic Microwave Background brightness divided by 10^3 for comparison, SZI is the thermal SZ effect for a cluster at rest with a comptonization parameter $y = 10^{-4}$ and SZII is the kinetic SZ effect for a cluster with $b = -10^{-4}$

2.3. Applications of the measurement of the SZ effects

The detection of the SZ distortions on the CMB toward clusters at a given redshift z_{cl} provides a lower limit to the redshift of origin of the CMB itself, $z_{cmb} > z_{cl}$, and gives a measure of the column density of the hot intracluster gas of electrons which is more direct than from the emission measure provided by the X-ray data.

Measurements realized at two or more frequencies give different linear combinations of y and b. Hence v_r can be measured, if the electronic temperature T_e is known (from X-ray data), from relationships (2) and (5):

$$v_r = \frac{kT_e}{m_e c^2} \frac{b}{y} c. \quad (8)$$

In particular, observations at $\nu = 217$ GHz ($\lambda = 1.38$ mm), where the thermal effect vanishes, could give a direct evaluation of the kinetic effect, which is usually smaller than the thermal one at other frequencies.

The combination of thermal SZ measurements and X-ray observations gives a powerful tool for the evaluation of the Hubble constant H_0, independent from the measurement of the distance of the cluster. The procedure described by Birkinshaw et al. (1991) is particularly illuminating. Nevertheless, for clusters with a peculiar velocity $v_r \sim 1000$ km/s, neglecting the contribution of the kinetic SZ effect in the calculations can lead to an over or underestimation of the Hubble constant by 20%.

2.4. SZ effects for unresolved clusters

When the cluster is unresolved, the total SZ effect over the whole cluster depends only on the cluster redshift and internal energy, which is proportional to the product of the mass by the temperature of the gas ($E_{int} \propto M_G \cdot T_e$). Knowing T_e (e.g.

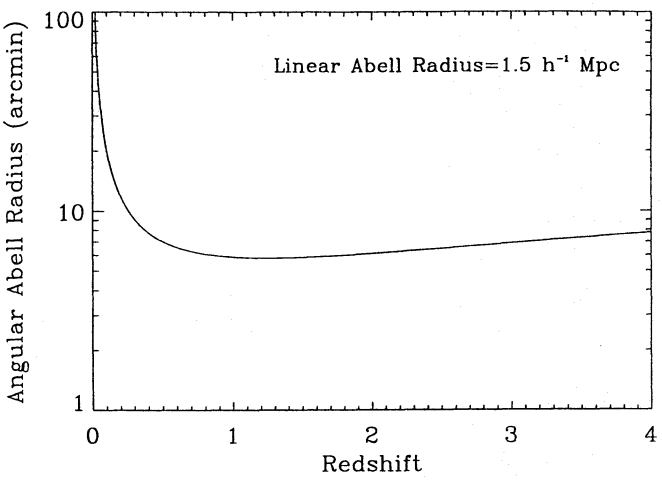

Fig. 2. The angular Abell radius 1.5 h^{-1}Mpc as a function of cluster redshift, calculated for $h = 0.5$ and $\Omega_0 = 1$ (density parameter). It represents an upper limit to the SZ extent of clusters

from X-ray data), a direct measurement of the total gas mass M_G in the cluster is obtained. Similarly, the kinetic effect of unresolved clusters depends only on the gas radial momentum ($P = M_G v_r$) relative to the CMB. In fact, the condition of unresolved cluster is satisfied for most of the low resolution experiments ($\theta_{FWHM} \geq 30$ arcmin). In Fig. 2, the typical Abell angular radius of a cluster is plotted as a function of redshift.

Calculations reported in Appendix A show that, assuming isothermality only (see relationship A6),

$$\int \frac{y\, d\Omega}{10^{-4}\ arcmin^2} = 0.43h^2 \left(\frac{M_G}{10^{14} M_\odot}\right)\left(\frac{kT_e}{10\ keV}\right)\frac{(1+z)^3}{(\sqrt{1+z}-1)^2} \quad (9)$$

where $\int y\, d\Omega$ is the measured quantity, z is the redshift and h is the Hubble constant normalized to 100 km/s/Mpc and a density parameter $\Omega_0 = 1$ is assumed. With additional reasonable assumptions (see Appendix A), we obtain the relationship between the monochromatic flux of a thermal SZ source, its total mass M and its redshift:

$$S_\nu = \psi(z)\, k_\nu\, M^{5/3} \quad (10)$$

where $\psi(z)$ and k_ν are functions specified in Appendix A.

Similarly, the monochromatic flux of a source of kinetic SZ effect depends only on its total mass, its redshift and its peculiar velocity:

$$S_\nu = v_r\, \phi(z)\gamma_\nu \cdot M \quad (11)$$

where $\phi(z)$ and γ_ν are functions specified in Appendix A.

As a consequence, for given cluster mass and velocity distributions, it is possible to construct the source counts. Note that considering sources as unresolved helps simplifying the calculations and makes them more general, in the sense that neither density distribution profiles have to be assumed nor clumpiness effects have to be taken into account.

3. Cluster velocity and mass distribution functions and the SZ source counts

3.1. Velocity distribution function

Several authors have developed N-body simulations to study the distribution of peculiar velocities of galaxy clusters in cosmological scenarios.

Recently, Croft & Efstathiou (1994) have calculated the theoretical peculiar velocity distributions in a low-density, cold dark matter universe (LCDM) with $\Omega_0 = 0.2$, cosmological constant $\Lambda = 3H_0^2(1-\Omega_0)$, and $h = 1$, and in a mixed dark matter universe (MDM) with $\Omega_{total} = 1$, $\Omega_\nu = 0.3$ and $h = 0.5$). In the LCDM model, the rms 3-dimensional peculiar velocity is $< v_{3D}^2 >^{1/2} = 415 \pm 5$ km/s, in the MDM model is $< v_{3D}^2 >^{1/2} = 751 \pm 12$ km/s: these values are compared to the predictions from linear perturbations theory which give $< v_{3D}^2 >^{1/2} = 391$ km/s for the LCDM model with $\sigma_8 = 1.0$ (σ_8 being the rms amplitude of the mass fluctuations in 8 h^{-1}Mpc) and $< v_{3D}^2 >^{1/2} = 711$ km/s for the MDM model with $\sigma_8 = 0.67$. The authors conclude that the distributions of the three-dimensional peculiar velocities resulting from the N-body simulations have more high peculiar velocity clusters than the Maxwellian distributions predicted by Gaussian statistics and are insensitive to the cluster richness and to the precise method used to identify clusters. Comparing their predictions to observational data, they show that the MDM model is marginally compatible with observations if the large errors on the peculiar velocities of the two clusters with $|v_{cmb}| > 2000$ km/s (Faber et al. 1989) are underestimated; the LCDM model gives a distribution narrower than the observed one [actually, Lucey et al. (1993) recently made new observations and found a value of the peculiar velocities of these two clusters - Abell 2199 and Abell 2634- considerably smaller than previous estimates ($v_p \sim 600 \div 700$ km/s)].

Rhee (1993) has developed N-body simulations to measure the amplitude and rms cluster peculiar velocity as a function of the bias parameter in HDM and CDM scenarios with $\Omega = 1$. He makes the hypothesis that inside a relaxed cluster of galaxies the velocity distribution will be Gaussian. N-body simulations are carried out assuming a Gaussian random density field, a linear theory and the Zel'dovich approximation. He finds a 3-dimensional rms peculiar motion of 211 km/s in a CDM universe with a bias factor of 1.5, increasing to 293 km/s for a bias factor of 1; in a HDM universe the values are respectively 205 km/s and 266 km/s. Even in these simulations, the calculated amplitudes of the cluster peculiar motion are in conflict with the observational claims of peculiar velocities of $\sim$ 2000 km/s. Rhee finds also that the growth rate of the peculiar velocity $v_p \propto R(t)$ (where $R(t)$ is the expansion parameter) is larger than that predicted by linear theory, in which the peculiar velocity is parallel to the peculiar force and $v_p \propto R(t)^{1/2}$.

On the basis of these considerations, if we accept the hypothesis that the primordial density fluctuations are Gaussian (Gaussian statistics), 3-dimensional peculiar velocities have a Maxwellian distribution. As we are interested in the *radial* velocity distribution, we must consider the 1-dimensional rms pe-

culiar velocity $< v_{1D}^2 >^{1/2} = \sigma_{0v}$. The 1-dimensional distribution is Gaussian and $\sigma_{0v} =< v_{3D}^2 >^{1/2} /\sqrt{3}$. Therefore, we opted for a Gaussian distribution of the cluster peculiar velocities in a linear theory scenario

$$f(v_r) = \frac{1}{\sigma_v(z)\sqrt{2\pi}} exp\left(-\frac{v_r^2}{2\sigma_v^2(z)}\right) \qquad (12)$$

satisfying the condition that $\int_{-\infty}^{+\infty} f(v_r)\, dv_r = 1$. According to the dependence of the growth rate of the peculiar velocity from the expansion parameter, as indicated by Rhee, we defined $\sigma_v(z) = \sigma_{0v} \cdot (1+z)^{-t}$, in which σ_{0v} is the cluster to cluster one-dimensional velocity dispersion at $z = 0$.

In the scenario of the linear theory the exponent t assumes the value $1/2$, nevertheless, we checked that a value of $t = 1$ only modifies counts for the faint SZ sources for which the dependence on the redshift is most important.

The value we choose for $\sigma_{0v} = 400$ km/s is on the high side of the results of the simulations mentioned above, but it is possible to show that a lower value of the rms peculiar velocity only shift counts (Figs. 4,5 and 6) to the left, without modifying the form of the curves (see later). Moreover, this value is in agreement with the simulation of the distribution of peculiar velocities of clusters in a CDM cosmological model ($\Omega_0 = 1$) by Bahcall, Cen and Gramann (1994).

3.2. Mass distribution function

We consider a Press-Schechter type mass function (hereafter PSMF), following BS (1994) and Peebles (1993), for the comoving number density of collapsed objects as a function of total mass M and redshift:

$$\frac{dN_c(z,M)}{dlnM} = \sqrt{\frac{2}{\pi}} \frac{\rho_0}{M} \nu_z(M) \left(-\frac{dln\Sigma}{dlnM}\right) e^{-\frac{\nu_z^2}{2}}. \qquad (13)$$

Here $\rho_0 = \Omega_0 h^2 \cdot 1.88\ 10^{-29}$g/cm^3 is the current mass density of the Universe, $\nu_z(M) = \delta_c(1+z)/\Sigma$, $\delta_c = 1.68$ and M is the total mass of the object. $\Sigma(M)$ is the current epoch, linearly-extrapolated power spectrum as a function of the mass scale and for a power law spectrum with exponent n is given by $\Sigma(M) = \Sigma_{15} M_{15}^{-\alpha}$, with $\alpha = (n+3)/6$, $M_{15} = M/10^{15} M_\odot$ and $\Sigma_{15} \sim 1/b$ (b: bias parameter).

In order to normalize the PSMF to experimental data, we compared the integral of expression (13), calculated from $M = 10^{12} M_\odot$ to infinity and for $z = 0$,

$$N_c(0, > M) = \int_M^\infty \frac{dN_c(0,M')}{dlnM'} dlnM'$$

to the integrated mass function of clusters of galaxies derived by Bahcall & Cen (1993, hereafter BC) from recent optical and X-ray observations (see Fig. 3):

$$N(> M)_{BC} = G_0 \frac{M^*}{M} exp\left(-\frac{M}{M^*}\right). \qquad (14)$$

Here $M^* = 0.18\ h^{-1} 10^{15} M_\odot$ and $G_0 = 4\ 10^{-5}$ h^{3}Mpc^{-3}. We adopted the parameters of PSMF corresponding to a flat CDM model with $n = -1$, $b = 1.7$, $\Omega_0 = 1$ and $h = 0.5$. As indicated by BC, flat CDM models with bias parameter $b \sim 2$ give, for the richest clusters, too steep a mass function and predict too many of them (Fig. 3): hence, we normalized the PSMF dividing it by the ratio $\eta = N_c(0, > M)/N(> M)_{BC} \sim 5$.

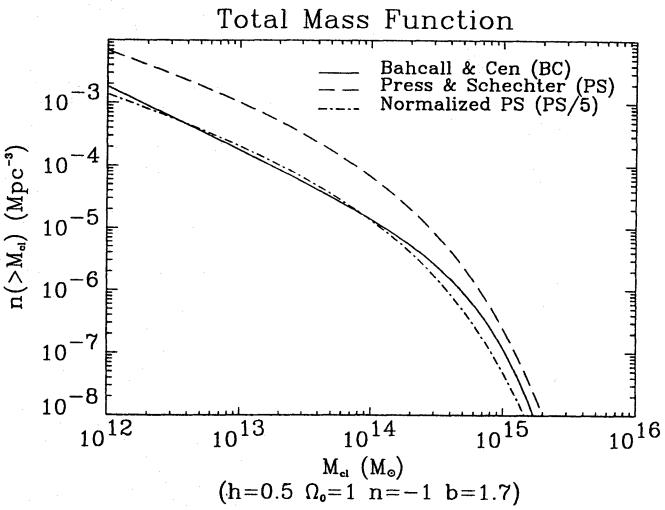

Fig. 3. The total mass function of clusters as a function of the total mass of a cluster M_{cl} in solar mass units. The theoretical model of Press-Schechter (dashed curve), resulting from the integration of the mass function (expression (13) in the text) between M_{cl} and infinity, is compared to the total mass function of Bahcall & Cen (1993) (solid curve) fitted to optical and X-ray data; the dashed-dot curve is the Press-Schechter function divided by 5 to be normalized to the fit of Bahcall & Cen

3.3. Construction of the LogN–LogS diagrams

The distribution of clusters per flux density interval, unit of redshift and solid angle (Ω, in steradian) is given by:

$$\frac{dN_{clu}}{dzd\Omega dlnS_\nu} = \frac{dN_c(z,S_\nu)}{dlnS_\nu} \cdot \frac{4c^3[\Omega_0 z + (\Omega_0 - 2)(\sqrt{\Omega_0 z + 1} - 1)]^2}{H_0^3 (1+z)^3 \Omega_0^4 (\Omega_0 z + 1)^{1/2}} \qquad (15)$$

where $dN_c(z,S_\nu)/dlnS_\nu$ is the comoving number density of sources per logarithmic interval of monochromatic flux. The relationship between the monochromatic flux, the mass and the redshift of a cluster, defined in the previous section, allows us to define the flux density distribution as a function of the mass density distribution (the details of calculations are given in Appendix B). Integrating over the redshift, we obtain the total number of thermal SZ sources per solid angle with flux greater than S_ν as:

$$N(> S_\nu) = \int_{S_\nu}^\infty \frac{dN_{clu}}{d\Omega dlnS_\nu} dlnS_\nu. \qquad (15')$$

In the case of the kinetic effect, the calculations are more complicated because of the dependence of the flux on the mass,

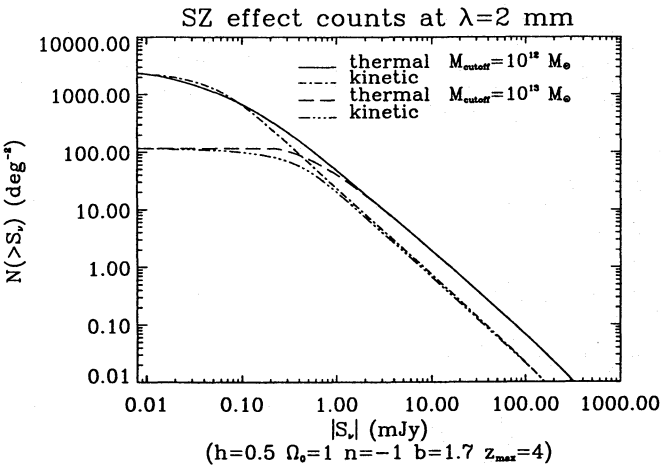

Fig. 4. The integral SZ source counts per unit solid angle at $\lambda = 2$ mm as a function of the absolute value of the flux of the SZ sources. The values of the parameters of the model are specified in the plot and in the text. M_{cutoff} indicates the minimum value of the mass of a source contributing to the SZ effects and is expressed in solar mass units. Solid and dashed lines are relative to the thermal SZ effect, for a mass cut off of $10^{12}M_\odot$ and $10^{13}M_\odot$ respectively; dot-dashed and dot-dot-dot-dashed curves are relative to the kinetic effect, for a mass cut off of $10^{12}M_\odot$ and $10^{13}M_\odot$ respectively

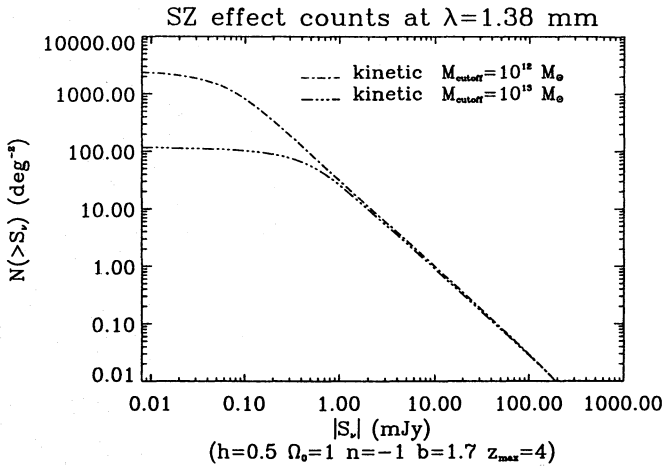

Fig. 5. The same as Fig. 4 for $\lambda = 1.38$ mm. Notice that only the kinetic SZ effect contributes to counts, the thermal effect being zero

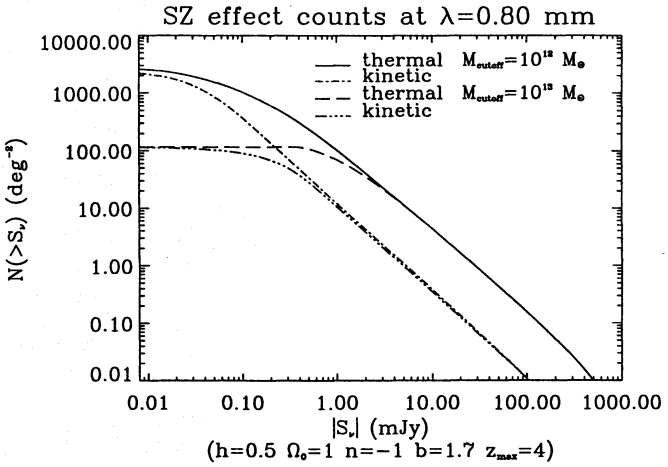

Fig. 6. The same as Fig. 4 for $\lambda = 0.80$ mm

the redshift *and* the velocity. The formalism we used to separate the variables is shown in Appendix B and gives the final expression:

$$N(>S_\nu) = 2\int_{S_\nu}^{\infty} S_\nu \int_0^{z'}\int_0^{+\infty} \frac{c}{H_0}\frac{(1+z)}{(\Omega_0 z+1)^{1/2}}\cdot$$

$$\frac{D_A^2(z)}{\phi(z)\gamma_\nu}\frac{f(v_r)}{v_r}\left[\frac{dN_c(z,M)}{dM}\left(M=\frac{S_\nu}{v\phi(z)\gamma_\nu}\right)\right] dvdzdlnS_\nu. \quad (16)$$

The factor 2 takes into account the fact that sources of either positive or negative flux, corresponding to negative or positive velocity respectively, contribute to the kinetic effect and our counts are taken for $|S_\nu|$.

4. Discussion of results

The counts, calculated at the three wavelengths $\lambda = 2$ mm, $\lambda = 1.38$ mm and $\lambda = 800$ μm, which are typical of the SZ effects (Fig. 1), are showed in Figs. 4, 5 and 6 respectively. First notice that counts at two wavelengths can be deduced from one another by a translation of the $ln|S_\nu|$ axis, which depends only on the two functions $f(x)$ and $a(x)$.

Source counts have been integrated only till $z' = 4$, but a higher limit does not change significantly the aspect of the curves. On the contrary, for $z' < 4$ the counts are sensibly reduced by at most the 30% for both the effects (see Figs. 7 and 8) at the lowest flux values.

Table 1. Values of the constant W in deg^{-2} of the functional dependence of $N(S_\nu)$ *vs* $|S_\nu|$ (see the text)

λ (mm)	*thermal*	*kinetic*
0.80	0.129	0.010
1.38	0.000	0.027
2.00	0.055	0.022

In order to define the minimum possible mass of a source contributing to the SZ effects, we put a cut off on the mass density distribution, M_{cutoff}, which in our model depends on the redshift as $M_{cutoff} = M_{min}(1+z)^3$. We considered the two cases of $M_{min} = 10^{12}M_\odot$ (corresponding to the mass of a small group of galaxies or a single large field galaxy) and $M_{min} = 10^{13}M_\odot$ (corresponding to the mass of small clusters). We can see that especially when the cut off is taken at $10^{12}M_\odot$ (Figs. 4, 5, 6) the contribution at low fluxes in the number of sources coming from the kinetic SZ effect is comparable to, or even larger than, the contribution coming from the thermal SZ

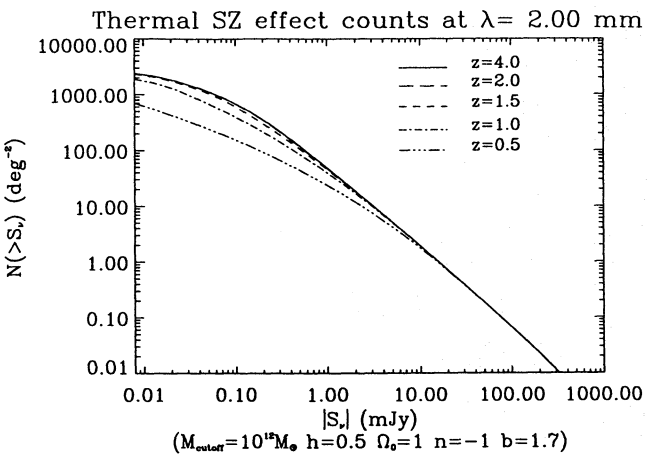

Fig. 7. The integral thermal SZ source counts per unit solid angle at λ = 2 mm as a function of the absolute value of the flux of the SZ sources and for different values of the redshift upper limit

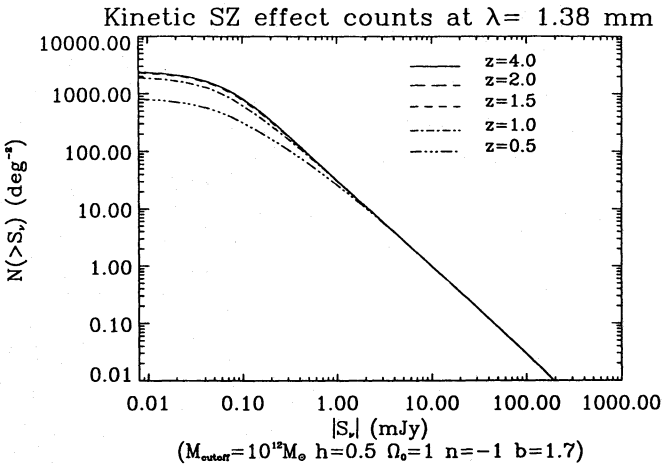

Fig. 8. The integral kinetic SZ source counts per unit solid angle at λ = 1.38 mm as a function of the absolute value of the flux of the SZ sources and for different values of the redshift upper limit

effect: this happens in particular for $S_\nu < 0.4$ mJy at $\lambda = 2$ mm and for $S_\nu < 0.1$ mJy at $\lambda = 800$ μm. The result is not surprising considering that small groups, having lower temperatures (smaller masses), are faint thermal SZ sources, but can show a kinetic SZ effect because their velocity dispersion in large potential wells is the same as big clusters.

The slope of the curves between 1000 and about 2 mJy confirms the euclidean approximation:

$$N(>S_\nu) = W\left(\frac{S_\nu}{100\ mJy}\right)^{-1.5} \qquad (17)$$

where the values of W are reported in Table 1.

In Appendix A we take the ratio of gas to total mass $g = M_G/M = 0.2$, following the discussion of White et al. (1993) for rich clusters (Coma), who indicate $M_G \sim 5.7 \cdot 10^{13}\mathrm{h}^{-5/2}\mathrm{M}_\odot$ and $M_{tot} \sim 6.7 \cdot 10^{14}\mathrm{h}^{-1}\mathrm{M}_\odot$. If we consider a value of g compatible with the nucleosynthesis constraints ($0.01 < \Omega_{baryonic}h^2 < 0.015$, Walker et al. 1991), all the curves in Figs. 4, 5 and 6 are shifted to the left by about a factor 10.

We choose $t = 0.5$ (see Sect. 3.1) compatible with the linear theory scenario. We calculated that a value of $t = 1$ only decreases the kinetic counts by $\sim 20\% \div 30\%$ for SZ fluxes $|S_\nu| < 0.5$ mJy. This limit is well below the flux sensitivity we considered for a typical 1m-class submillimeter space experiment (see below), so that our present results do not significantly depend on the value of the t parameter.

Future space experiments will reach a sensitivity of about 100 mJy at 3σ in the range of wavelengths of 800 μm$< \lambda < 2$ mm and then could observe about 4000 thermal SZ sources and 1000 kinetic SZ sources over the whole sky, according to the logN-logS counts. Integral count plots give us an idea of the confusion limits for thermal and kinetic SZ sources in the case of a 1-m class experiment (D (antenna diameter)=1 m) by the formula $N(>S_{\nu,lim})\cdot\Omega_{instr} > 1/25$, where $\Omega_{instr} = (1.22\lambda/D)^2\cdot\pi/4$ is the instrument solid angle. Calculations show that for both effects $S_{\nu,lim} < 10$ mJy at all wavelengths, an order of magnitude less than the typical sensitivity we considered. Likewise, we followed the formalism used by Fischer and Lange (1993) to calculate the confusion limits by other sources to the measurement of the SZ effect at millimeter wavelengths: we found that for a typical experiment of 10 arcmin resolution, radio sources and infrared galaxies give a confusion limit less than 10 mJy at the three wavelengths we considered. The contribution of IRAS cirrus would be particularly important at 0.8 mm (some hundreds of mJy) in regions where the average 100 μm brightness of the dust emission is greater than 5 MJy, so that shorter wavelength channels would be necessary to subtract the contribution of the dust.

We also compared the integral counts to the calculations of Franceschini et al. (1991) of galaxy counts at millimetric wavelengths. We obtained that for values of flux greater than 40 mJy the number of thermal SZ sources per square degree is greater by about an order of magnitude than that of galaxies at $\lambda = 0.8$ mm. The same happens in the case of the kinetic effect comparing to galaxy counts at $\lambda = 1.3$ mm and for fluxes greater than about 10 mJy.

Source counts allow us also to evaluate the average comptonization parameter, independent of frequency and calculated as

$$\overline{y} = \frac{1}{B_{\nu,cmb}\,|f(x)|}\int_0^{S_\nu max} S_\nu \frac{dN_{clu}}{d\Omega dlnS_\nu}\, dlnS_\nu \qquad (18)$$

We obtained a $\overline{y} = 1.2 \cdot 10^{-6}$, consistent with the result of the simulations by Markevitch et al. (1992) for the evaluation of the fluctuations of the CMB from clusters of galaxies ($\overline{y} \sim 10^{-6}$ for models with $\Omega_0 = 1$). Our result is also compatible with the level given by COBE, $|y| < 2.5\ 10^{-5}$ (95 % confidence level, Mather et al. 1994).

4.1. Evaluation of the brightness and temperature r.m.s. fluctuations

Thermal and kinetic SZ source counts can also be used in order to evaluate their contribution to the r.m.s. relative CMB brightness fluctuations $\delta B_\nu / B_{\nu,cmb}$ and $\delta T / T_{cmb}$ of the CMB at that frequency.

These quantities depend on the instrument beam θ_{beam} and can be computed as follow:

$$\left(\frac{\delta B_\nu}{B_{\nu,cmb}}\right)_{rms} = \frac{1}{B_{\nu,cmb}} \cdot \left[\int_{S_\nu min}^{S_\nu max} \frac{1}{\Omega} \cdot S_\nu^2 \frac{dN_{clu}}{d\Omega dlnS_\nu}\, dlnS_\nu\right]^{\frac{1}{2}} \quad (19)$$

where $B_{\nu,cmb}$ is the CMB brightness at frequency ν, $dN_{clu}/d\Omega dlnS_\nu$ is given by the integration over the redshift of the expression (15) for the thermal effect and by the analogous expression for the kinetic effect, and $\Omega = \pi\theta_{beam}^2/4$ is the solid angle corresponding to the instrument beam.

The corresponding rms Comptonisation parameter is given by:

$$y_{rms} = \left(\frac{\delta B_\nu}{B_{\nu,cmb}}\right)_{rms} \cdot \frac{1}{|f(x)|}. \quad (20)$$

We calculated its value for the beam corresponding to the diffraction limit of a 1 m-class experiment and we obtained $y_{rms} = 6.5 \cdot 10^{-7}$ for $\lambda = 2$ mm and $y_{rms} = 1.35 \cdot 10^{-6}$ for $\lambda = 800$ μm.

In order to evaluate the r.m.s. thermodynamic temperature fluctuations for both effects, we used the relationship:

$$\left(\frac{\delta T}{T}\right)_{rms} = \frac{e^x - 1}{xe^x} \cdot \left(\frac{\delta B_\nu}{B_{\nu,cmb}}\right)_{rms} \quad (21)$$

where x has the same meaning as in the expression (1) and T is the average thermodynamic temperature of the CMB.

All the numerical examples which follow have been computed for a typical 1 m-class space experiment with three channels centered at 2 mm, 1.38 mm and 800 μm. $S_\nu min$ is arbitrarily taken to be 1 μJy, but the results do not depend much on this value. The value of $S_\nu max$ corresponds to the flux sensitivity of the experiment: the fluctuations computed are due to sources below this threshold, thus undetected as individual sources. In Fig. 9, we show the dependence of the rms temperature fluctuations on this threshold at an angular scale of 10 $arcmin$: the fluctuations depend on the upper limit of the integral in the expression (19) as

$$\frac{\delta T}{T_{cmb}} = G_{100} \cdot \left(\frac{S_\nu max}{100\ mJy}\right)^{1/3} \quad (22)$$

where $G_{100} \sim 8 \cdot 10^{-7}$ and $G_{100} \sim 2 \cdot 10^{-6}$ respectively at 2 mm and at 800 μm for the thermal effect and $G_{100} \sim 5 \cdot 10^{-7}$ for the kinetic effect (valid for $S_\nu max > 10$ mJy). We have taken $S_\nu max \sim 100$ mJy which represents a typical sensitivity at 3σ of future space experiments.

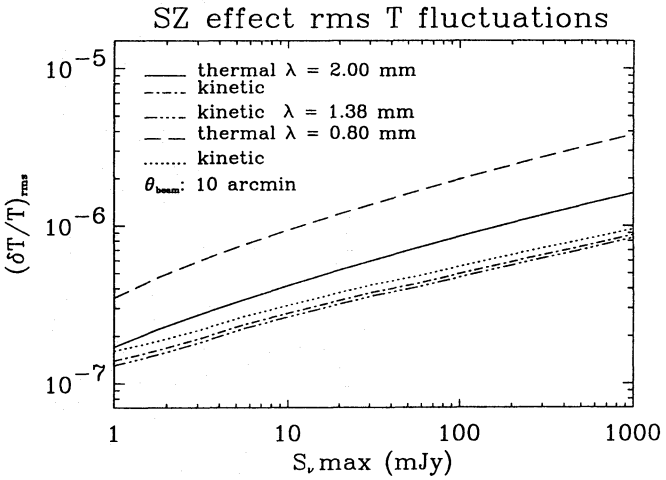

Fig. 9. The rms temperature fluctuations for the thermal and kinetic SZ effects represented as a function of the flux upper limit. Calculations are plotted for the three wavelengths of previous figures and for a typical beam aperture of 10 arcmin. The functional dependence is quite the same for the five curves, except for the absolute level. The dependence on the beam is given by equation (20)

Table 2. Values of the constant C_{10} in 10^{-7} of the functional dependence of SZ $\frac{\delta T}{T}$ vs θ_{beam} (formula 23)

λ (mm)	*thermal*	*kinetic*
0.80	20.0	~ 4.0
1.38	0.00	~ 4.0
2.00	8.50	~ 4.0
radio ($>$ 10 cm)	16.0	~ 5.0

In the case of the kinetic SZ effect, the sources cannot be spectrally distinguished from the primary anisotropies (the effect is constant at all frequencies when expressed in $\delta T/T$ form, see Fig. 10). We assumed, as a first statistically valid approximation, that the number of clusters that can be identified by the thermal SZ effect sources can be used to define the $S_\nu max$ for the kinetic SZ effect. As a consequence, we compute from counts the $S_\nu max$ associated to a number of kinetic sources equal to the number of thermal sources at $S_\nu max \sim 100$ mJy. We found a value of approximately $S_\nu max \sim 40$ mJy, at 2 mm and 1.38 mm, and $S_\nu max \sim 20$ mJy at 800 μm. The rms thermodynamic temperature fluctuations due to the kinetic effect represented in Fig. 10 are calculated for $S_\nu max \sim 40$ mJy. Nevertheless, if an experiment has no way to spectrally identify thermal SZ sources (for example a one frequency experiment) one must consider the contribution to the integral of all sources up to $S_\nu max \sim 1$ Jy for both the effects. In Fig. 10 we also plotted the results for this case. As we can see, the level of the kinetic SZ effect temperature fluctuations is augmented only by a factor of 2.2.

Once the integration limits are fixed, expressions (19) and (21) imply that $\delta T/T$ depends on θ_{beam} following the relation-

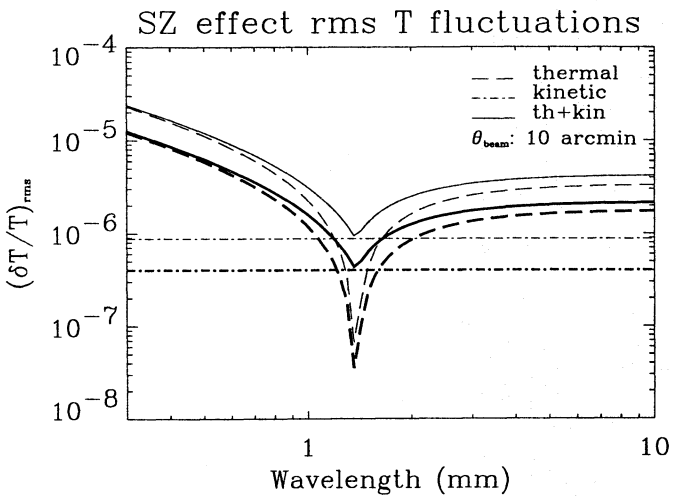

Fig. 10. The rms temperature fluctuations for the thermal and kinetic SZ effects represented as a function of the wavelength. The dashed lines refer to the thermal effect and are calculated separately for two flux limits, as indicated in the text (thinner line: $S_\nu max$ = 1000 mJy; thicker line: $S_\nu max$ = 100 mJy). Likewise, the kinetic effect for two values of the flux limits (thinner line: $S_\nu max$ = 1000 mJy; thicker line: $S_\nu max$ = 40 mJy, see the text) is represented by the dot-dashed curves. The solid lines show the rms temperature fluctuations for the sum of the two effects. The typical beam amplitude used is of 10 arcmin. The range of wavelengths in which the kinetic effect dominates on the thermal one is roughly between 1.2 and 1.6 mm for the two different values of the flux upper limit

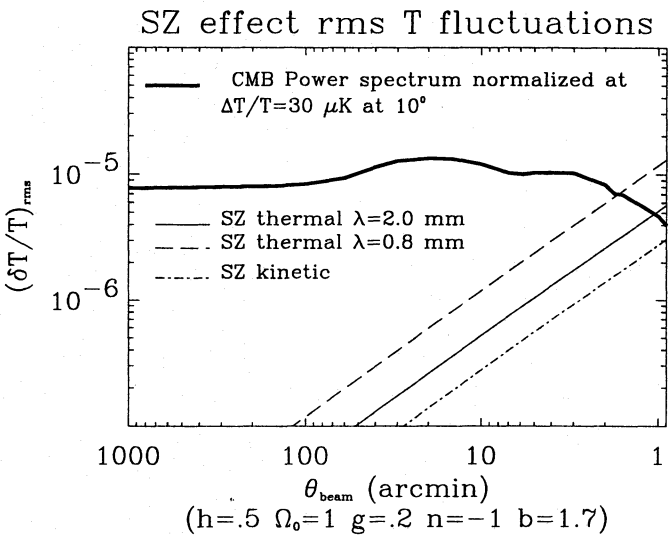

Fig. 11. The rms temperature fluctuations for the thermal and kinetic SZ effects represented as a function of the angular scale. Solid and dashed curves indicate the thermal SZ effect for the different wavelengths specified in the figure (λ = 2.00 mm and λ = .80 mm respectively); the dot-dashed curve indicates the kinetic SZ contribution at all wavelengths. The solid curve labeled CMB is the CMB power spectrum normalized to COBE at $\Delta T/T$ = 30 μK at 10° (Melchiorri 1993). The contribution of both effects becomes significant at angular scales smaller than 20 arcmin

ship:

$$\frac{\delta T}{T_{cmb}} = C_{10} \cdot \left(\frac{\theta}{10\ arcmin}\right)^{-1} \qquad (23)$$

where the values of the constant C_{10} for both effects and at the three wavelengths are shown in Table 2 (calculations for $\lambda > 10$ cm are made considering a flux sensitivity of 80 μJy). We stress the fact that, as expected, the SZ thermal effect vanishes at λ = 1.38 mm, the SZ kinetic effect, on the contrary, still contributes to the counts (Fig. 5) and, as a consequence, to the fluctuations of the CMB. More specifically, the kinetic SZ effect remains larger than the thermal SZ effect in the range of wavelengths 1.2 mm$< \lambda \leq$ 1.6 mm (Fig. 10). The level of these fluctuations is of about 10^{-6} for the thermal effect and of the order of $\sim 3 \cdot 10^{-7}$ for the kinetic effect. Future experiments characterized by a high sensitivity in the (sub)millimetric or radio domain cannot neglect the contribution of these backgrounds any more.

In Fig. 11 the rms temperature fluctuations of the SZ effects are compared to the square root of the CMB power spectrum normalized to COBE results ($\Delta T/T$ = 30 μK at an angular scale of 10 degrees) and calculated for Ω_0 = 1, g = 0.2 and h = 0.5. This comparison is possible only if we want to consider the result of differential observations made by an ideal experiment with a pencil beam. This condition is verified if we make the approximation that all the considered sources are point sources. At scales smaller than 10 arcmin this approximation starts to break down. Moreover, clustering of clusters cannot be neglected. Simulations are being developed for this case and will be discussed in a future paper; the fluctuation level will not increase as fast at small angular scales. We note that a simple measurement of the level of the primordial anisotropies at scales around 30 arcmin will not be affected much by the thermal and kinetic SZ effect temperature fluctuations. On the other hand, a detailed study of the caracteristics of the power spectrum with a high signal/noise ratio of, e.g., $S/N \sim 10$ should not neglect the additional contribution of these fluctuations, especially in the range 3 to 20 arcmin.

5. Conclusion

Future satellites, devoted to the observation of infrared and submillimeter backgrounds, will be able to detect some thousands of thermal and kinetic SZ sources. The measurement of the peculiar velocity of hundreds of clusters could provide a unique way of probing the distribution of matter on very large scales. The contribution of both thermal and kinetic SZ sources to the diffuse backgrounds in terms of CMB temperature fluctuations cannot be neglected in very high sensitivity experiments at small angular scales ($\Delta T/T \sim 10^{-6}$, $\theta_{beam} < 10$ arcmin). Our calculations of the mean flux from thermal SZ effect sources give an estimate of the Comptonization parameter $\overline{y} = 1.2 \cdot 10^{-6}$ which is compatible with the level set by COBE and consistent with the results of other similar simulations.

Appendix A: calculation of the thermal and kinetic SZ source flux as a function of the total mass, the redshift and the peculiar velocity

Generally, the gas mass of a cluster M_G is given by:

$$M_G = \int\int\int m_p \mu\, n_e\, dl\, d\chi\, d\zeta \qquad (A1)$$

where m_p is the proton mass, μ is a factor that takes into account the presence of protons and ionized He atoms ($\mu = (1+y')/(1+y'/2)$; $y' = 4n_{He}/n_H \sim 23\%$), n_e is the numerical density of electrons, χ and ζ are the coordinates on the celestial plane of the cluster and l is the line of sight. In this expression, the $\int\int d\chi d\zeta$ is related to the solid angle, Ω, and the angular distance of the source, $D_A(z)$, depending on the redshift:

$$\int\int d\chi\, d\zeta = D_A^2(z) \int_\Omega d\Omega \qquad (A2)$$

where

$$D_A^2(z) = \frac{4c^2}{H_0^2}\left[\frac{\Omega_0 z + (\Omega_0 - 2)(\sqrt{\Omega_0 z + 1} - 1)}{\Omega_0^2 (1+z)^2}\right]^2 \qquad (A3)$$

(H_0 is the Hubble constant and Ω_0 is the density parameter). The integral of the electronic numerical density over the line of sight is related to the SZ distortion by means of the optical depth τ:

$$\int_l n_e\, dl = \frac{\tau}{\sigma_T}. \qquad (A4)$$

We obtain:

$$M_G = m_p \mu \int_\Omega \frac{\tau}{\sigma_T} D_A^2(z)\, d\Omega \qquad (A5)$$

where, in the case of the *thermal* SZ effect, $\tau = y\, m_e c^2/(kT_e\sigma_T)$. For an unresolved cluster, the SZ measurement is relative to the whole cluster and is proportional to $f_y = \int_\Omega y\, d\Omega$. Substituting in the previous expression

$$M_G = m_p \mu \frac{m_e c^2}{kT_e \sigma_T} D_A^2(z)\, f_y \qquad (A6)$$

f_y is related to the monochromatic flux S_ν of the SZ distortion, which is given by:

$$S_\nu = \int_\Omega \Delta B_\nu d\Omega = \int_\Omega B_{\nu,cmb}\, y\, f(x) d\Omega. \qquad (A7)$$

That means:

$$f_y = \frac{S_\nu}{B_{\nu,cmb} f(x)}. \qquad (A8)$$

If we substitute in the (A6) we find the expression of the gas mass of the cluster as a function of the flux:

$$M_G = m_p \mu \frac{m_e c^2}{kT_e \sigma_T} D_A^2(z) \frac{S_\nu}{B_{\nu,cmb} f(x)}. \qquad (A9)$$

Hence the intracluster gas mass is directly related to observable quantities: its temperature, the cluster redshift and the total flux density.

The virial temperature of the intracluster gas is a function of the total mass, as indicated by Kaiser (1986) for a self-similar ICM (Intra Cluster Medium) in a flat Universe and specified by BS (1994):

$$T_e = T_{15}\left(\frac{M}{M_{15}}\right)^{2/3}(1+z) \qquad (A10)$$

where $M_{15} = 10^{15}\, M_\odot$. A possible normalization is indicated by Evrard (1990, cited on BS) by means of hydrodynamic simulations, $kT_{15} = 6.4 \cdot h^{2/3}$keV. Moreover, we define the ratio between the mass of the intracluster medium, M_G, and the total mass of a cluster M (baryonic and non-baryonic) by $g = M_G/M$. Using the values indicated by White et al. (1993) for the Coma cluster, we consider $g \sim 0.2$ and we substitute in the previous expression to obtain an expression for the total mass of a cluster:

$$M = \left(\frac{S_\nu}{\psi(z) k_\nu}\right)^{3/5}. \qquad (A11)$$

Here

$$\psi(z) = \frac{g \sigma_T k T_{15}(1+z)}{m_p \mu\, m_e c^2\, D_A^2(z) M_{15}}$$

and

$$k_\nu = B_{\nu,cmb} f(x).$$

In the case of the *kinetic* SZ effect, $\tau = b/\beta$. Following similar considerations, we will have:

$$M_G = m_p \mu \frac{c}{v_r \sigma_T} D_A^2(z) \int_\Omega b\, d\Omega \qquad (A12)$$

which gives

$$M_G = m_p \mu \frac{c}{v_r \sigma_T} D_A^2(z)\, f_b. \qquad (A13)$$

Note that contrary to the thermal SZ effect we do not assume isothermal medium. If we define

$$f_b = \int_\Omega b\, d\Omega = \frac{S_\nu}{B_{\nu,cmb} a(x)}$$

the total mass of the cluster will be given by:

$$M = \frac{S_\nu}{v_r\, \phi(z) \gamma_\nu} \qquad (A14)$$

where

$$\phi(z) = \frac{g \sigma_T}{m_p \mu\, c\, D_A^2(z)}$$

and

$$\gamma_\nu = B_{\nu,cmb} a(x).$$

Appendix B: relationship between the flux density distribution and the mass density distribution

The expression (15) can be expressed as a function of the angular distance, the redshift and the mass distribution function to obtain:

$$\frac{dN_{clu}}{dzd\Omega dlnS_\nu} = \frac{3}{5}\frac{dN_c(z,M)}{dlnM}\frac{c}{H_0}\frac{(1+z)}{\sqrt{\Omega_0 z+1}}D_A^2(z). \quad (B1)$$

We considered from expression (A11) that

$$\frac{dN_c(z,S_\nu)}{dlnS_\nu} = \frac{3}{5}\frac{dN_c(z,M)}{dlnM}.$$

For the kinetic effect we have to separate the dependence of the flux from the mass and the velocity. The mass distribution is taken at the value for which (A14) is satisfied, hence the cluster distribution in redshift, solid angle, flux, velocity and mass can be written:

$$\frac{dN_{clu}}{dzd\Omega dS_\nu dv_r dM} = \frac{c}{H_0}\frac{(1+z)}{\sqrt{\Omega_0 z+1}}\cdot$$

$$D_A^2(z)\, f(v_r)\, \frac{dN_c(z,M)}{dM}\delta(S_\nu - Mv_r\phi(z)\gamma_\nu) \quad (B2)$$

where $dN_c(z,M)/dM$ is given by the relationship (13) and δ is the Dirac distribution. After a change of variables we find:

$$\frac{dN_{clu}}{dzd\Omega dS_\nu dv_r} = \frac{c}{H_0}\frac{(1+z)}{\sqrt{\Omega_0 z+1}}\cdot$$

$$\frac{D_A^2(z)}{\phi(z)\gamma_\nu}\frac{f(v_r)}{v_r}\left[\frac{dN_c(z,M)}{dM}\left(M=\frac{S_\nu}{v_r\phi(z)\gamma_\nu}\right)\right]. \quad (B3)$$

References

Bahcall, N.A., Cen, R., 1993, ApJ, 407, L49

Bahcall, N.A., Cen, R., Gramann, M., 1994, ApJ, 430, L13

Bartlett, J., Silk, J., 1994, ApJ, 423, 12

Bernardeau, F., 1993, What can we learn from the large-scale velocity field?. In: Bouchet F., Lachièze-Rey M. (eds.) Proc. 9^{th} IAP Astrophysics Meeting, Cosmic Velocity Fields. Editions Frontières, Paris (France), p. 285

Birkinshaw, M., 1991. In: Trân Than Vân J. (ed.) Physical Cosmology. Editions Frontières, Gif sur Yvette, France

Birkinshaw, M., Gull, S.F., Northover, K.J.E., 1978, MNRAS, 185, 245

Birkinshaw, M., Gull, S.F., Moffet, A.T., 1981a, ApJ, 251, L69

Birkinshaw, M., Gull, S.F., Northover, K.J.E., 1981b, MNRAS, 197, 571

Birkinshaw, M., Gull, S.F., Hardebeck, H., 1984, Nat, 309, 34

Birkinshaw, M., Hughes, J.P., Arnaud, K.A., 1991, ApJ, 379, 466

Cavaliere, A., Colafrancesco, S., Menci, N., 1993, ApJ, 415, 50

Cavaliere, A., Menci, N., Setti, G., 1991, A& A, 245, L21

Croft, R.A.C., Efstathiou, G. 1994, MNRAS, 268, L23

Dekel, A., 1993, Determining Ω from peculiar velocities. In: Bouchet F., Lachièze-Rey M. (eds.) Proc. 9^{th} IAP Astrophysics Meeting, Cosmic Velocity Fields. Editions Frontières, Paris (France), p. 157

De Luca, A., Bernard, J.P., Désert, F.X., et al., 1993, PRONAOS-SPM: a Balloon-borne Experiment Well Adapted to Measure the Short Wavelength Part of the Sunyaev-Zel'dovich Effect. In: Seitter W. (ed.) Proc. NATO-ASI, Cosmological Aspects of X-ray Clusters of Galaxies, Kluwer, Dordrecht, p. 247

Désert, F.X., De Luca, A., Lamarre, J.M., Puget, J.L., 1993, How to Measure Peculiar Velocity Fields on a Very Large Distance Scale. In: Bouchet F., Lachièze-Rey M. (eds.) Proc. 9^{th} IAP Astrophysics Meeting, Cosmic Velocity Fields. Editions Frontières, Paris (France), p. 541

Evrard, A.E., 1990. In: Fitchett M., Oegerle W. (eds.) Clusters of Galaxies. Cambridge University Press, Cambridge

Faber S., Wegner, G., Burstein D., et al., 1989, ApJS, 69, 763

Fischer, M.L., Lange, A.E., 1993, ApJ, 419, 433

Fischer, M.L., Ho, T.R., Holzapfel, W.L., et al., 1993, preprint

Franceschini, A., Toffolatti, L., Mazzei, P., Danese, L., and De Zotti, G., 1991, A& AS, 89, 285

Grainge, K., Jones, M., Pooley, G., Saunders, R., Edge, A., 1993, MNRAS, 265, L57

Jones, M., Saunders, R., Alexander, P., et al., 1993, Nat, 365, 320

Kaiser, N., 1986, MNRAS, 222, 323

Korolev, V.A., Sunyaev, R.A., Yakubtsev, L.A., 1986, SvA, 12(3), L141

Lamarre, J.M., Pajot, F., Torre, J.P., et al., 1994, Infr. Phys. Technol., 35, 277

Lauer, T.R., Postman, M., 1994, ApJ, 425, 418

Lucey, J.R., Guzman, R., Steel, J., Carter, D., 1993, Abell 2199 and Abell 2634 Revisited. In: Bouchet F., Lachièze-Rey M. (eds.) Proc. 9^{th} IAP Astrophysics Meeting, Cosmic Velocity Fields. Editions Frontières, Paris (France), p. 43

Mandolesi, N., Bersanelli, M., Cesarsky, C., Danese, L., Efstathious, G., Griffin, M., Lamarre, J.M., Norgaad-Nielsen, H.U., Pace, O., Puget, J.L., Raisanen, A., Smoot, G.F., Tauber, J., Volonté, S., 1994, COBRAS-SAMBA: the ESA Medium Size Mission for Measurements of CBR Ansotropy. In: Dust, Molecules and Backgrounds, Capri 1994 Workshop

Markevitch, M., Blumenthal, G.R., Forman, W., Jones, C., Sunyaev, R.A., 1992, ApJ, 395, 326

Mather, J.C., Cheng, E.S., Cottingham, D.A., et al., 1994, ApJ, 420, 439

Melchiorri, F., 1993, Potential problems: Primordial LiH, very cold dust. In: First Meeting for the SAMBA missions, Orsay, December 16th 1993

Peebles, P.J.E., 1980. In: The Large-Scale Structure of the Universe. Princeton University Press, Princeton

Peebles, P.J.E., 1993. In: Principles of Physical Cosmology. Princeton University Press, Princeton

Puget, J.L., 1993. Proposal in answer to the call for mission ideas for the next medium size project (M3) of the European Space Agency

Rephaeli, Y., Lahav, O., 1991, ApJ, 372, 21

Rhee, G., 1993, ApJ, 411, 455

Sunyaev, R.A., Zel'dovich, Ya.B., 1970, Ap& SS, 7, 3

Sunyaev, R.A., Zel'dovich, Ya.B., 1970, Comments Astrophys. Space Phys., 4, 173

Sunyaev, R.A., Zel'dovich, Ya.B., 1980, MNRAS, 190, 413

Vishniac, E.T., 1987, Ap.J., 322, 597

Walker, T.P., Steigman, G., Schramm, D.N., Olive, K.A., and Kang, H.-S., 1991, ApJ, 376, 51

White, D.M., Navarro, J.F., Evrard, A.E., Frenk, C.S., 1993, Nat, 366, 429

Wilbanks, T.M., Ade, P.A.R., Fischer, M.L., Holzapfel, W.L., Lange, A.E., 1994, ApJ, 427, L75

This article was processed by the author using Springer-Verlag LaTeX A&A style file version 3.